Materials Transactions, Vol. 57, No. 9 (2016) pp. 1424 to 1432
Special Issue on Advanced Materials Science in Bulk Nanostructured Metals III

Three-Dimensionally Gradient and Periodic Harmonic Structure for High Performance Advanced Structural Materials

Sanjay Kumar Vajpai[1,*], Han Yu[2], Mie Ota[3,*], Ikumu Watanabe[4,*], Guy Dirras[5] and Kei Ameyama[3,*]

[1]*Research Organization of Science and Technology, Ritsumeikan University, Kusatsu 525–8577, Japan*
[2]*Graduate School, Ritsumeikan University, Kusatsu 525–8577, Japan*
[3]*Department of Mechanical Engineering, Ritsumeikan University, Kusatsu 525–8577, Japan*
[4]*National Institute for Materials Science, Tsukuba 305–0047, Japan*
[5]*Université Paris 13, Sorbonne Paris Cité, LSPM-CNRS, France*

Creation of a unique "Harmonic Structure (HS)" with controlled bimodal grain size distribution in metals and alloys is a new material design paradigm allowing the improved mechanical performance of structural materials via enhancing strength without sacrificing ductility. A well designed powder metallurgy based processing approach has been developed to create such a controlled microstructure which consists of controlled mechanical milling (MM) of powder particles to create powder particles with bimodal grain size distribution, with a peculiar core-shell structure, followed by their hot consolidation. In the present study, full density compacts with HS were prepared and the effect of such a bimodal microstructure on the mechanical properties of commercially pure Ti with hexagonal close packed (HCP) crystal structure was investigated. The HS pure Ti exhibited considerably higher strength values, without sacrificing ductility, as compared to their coarse-grained (CG) counterparts. The numerical simulation results revealed that the initial stages of deformation and strength of the HS are governed by the characteristics of the interconnected network of the strong fine-grained (FG) shell regions whereas the extent of uniform deformation and overall ductility is governed by the ductile CG core region. It was also demonstrated that the unique HS design promotes uniform deformation very efficiently by avoiding strain localization during plastic deformation. [doi:10.2320/matertrans.MH201509]

(Received March 1, 2016; Accepted April 4, 2016; Published May 13, 2016)

Keywords: *harmonic structure, powder metallurgy, bimodal Titanium, lightweight materials, severe plastic deformation, strengthening*

1. Introduction

Strengthening of structural materials via microstructural manipulations is an efficient strategy of preparing lightweight materials with improved properties and performance. Especially, microstructural refinement, such as grain refining, has emerged as an attractive method of achieving high strengths in most of the metallic structural materials.[1–3)] The strengthening via microstructural refinement provides an opportunity to prepare lightweight and miniaturized components of the currently used commercial metals and alloys without compromising performance. Particularly, grain refinement in metals and alloys is an effective method to achieve manifold increments in the strength. Especially, materials having submicron-sized ultrafine-grained (UFG) structure and nano-grained (NG) structure have demonstrated the possibility of achieving exceptionally high strength values. A variety of novel processes based on severe plastic deformation (SPD) have been developed for the preparation bulk UFG and nano-grained (NG) materials. The major processing routes to prepare bulk UFG and NG materials include High Pressure Torsion (HPT), Accumulative Roll Bonding (ARB), Equal Channel Angular Pressing/Extrusion (ECAP/ECAE), Cryogenic Rolling, Multiaxial Forging, Repetitive Corrugation and Straightening, and Powder Metallurgy (PM) based process consisting of ball milling of powders followed by their consolidation.[3–10)] It would be worth mention that these processes resulted in bulk materials with "homogeneous" UFG and NG microstructures, which exhibited extremely high strengths as compared to their CG counterparts. However, these bulk homogeneous UFG/NG materials had extremely poor ductility as compared to their CG counterparts. Therefore, unfortunately, the homogeneous UFG/NG microstructures did not led to improved strength-ductility combination, i.e. toughness, which is an important parameter for gauging the enhanced performance in structural materials.

In recent years, it has been demonstrated that the materials with bimodal grain size distribution exhibit high strength together with high ductility.[11–14)] The initial work on the creation of bimodal microstructures in bulk materials was based on the conventional ingot metallurgy route consisting of severe plastic deformation followed by controlled heat-treatment. However, the major drawback of such a processing methodology is the lack of precise control over the various important parameters of the bimodal microstructure such as grain size, UFG/CG volume fraction, and spatial distribution of UFG and CG areas, leading to a large scatter in the mechanical properties. Obviously, such a large scatter in the mechanical properties makes these bulk materials extremely unreliable for most of the practical applications. Therefore, there is a need to make efforts to develop new ways of preparing bulk materials with controlled bimodal microstructure to achieve reliable mechanical properties and performance.

In an effort to deal with the issue of controlled heterogeneous microstructure, Ameyama and co-workers proposed and developed bulk structural materials with a unique controlled microstructural design, called "Harmonic Structure", having bimodal grain size distribution.[15–20)] The harmonic structure is a heterogeneous bimodal microstructure with a controlled and specific topological distribution of fine and coarse grains, i.e. the CG areas ("core") embedded as islands in the matrix of three-dimensional continuously connected network ("shell") of UFG areas (Fig. 1). However, it would be

*Corresponding author, E-mail: vajpaisk@gmail.com, mie-ota@fc.ritsumei.ac.jp, watanabe.ikumu@nims.go.jp, ameyama@se.ritsumei.ac.jp

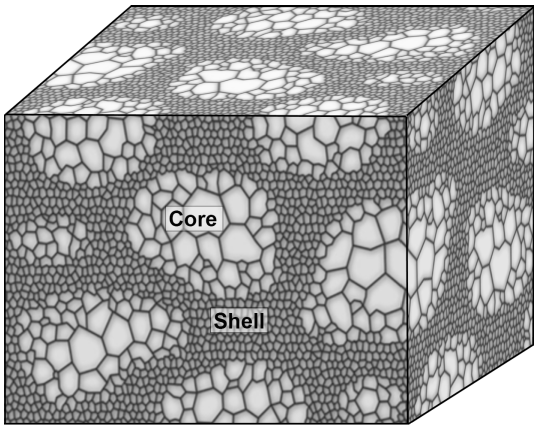

Fig. 1 An schematic diagram illustrating the harmonic structure design.

worth mention that the harmonic structure is heterogeneous on micro- but homogeneous on macro-scales. Furthermore, an efficient and novel powder metallurgy (PM) processing route was also developed to prepare bulk materials with such a strictly controlled microstructure. The carefully designed proposed PM method involved achieving deformed powder particles with bimodal grain size distribution via controlled plastic deformation of powder particles. Subsequently, consolidation of these deformed powder particles results in bulk material with harmonic structure.

It would be worth mentioning that the majority of the previous work on the creation and evaluation of harmonic structure design dealt with the metals and alloys with cubic crystal structure, and only a very small amount of preliminary work is available dealing with the commercially important metals and alloys with hexagonal close-packed (HCP) crystal structure. A preliminary work was carried out on the application of the harmonic structure design to pure Ti owing to the fact that pure Ti and its alloys with hexagonal close packed (HCP) crystal structure are one of the important classes of structural materials.[15,18] Although the harmonic-structured pure Ti exhibited superior mechanical properties as compared to its homogeneous fine-/coarse-grained counterparts, the scope of the preliminary work was limited only to the creation of harmonic structured pure Ti and evaluation of its mechanical properties. The study did not elaborate the effect of harmonic structure on the deformation behavior on the resulting bulk material. Moreover, there were some issues related with the processing and control over microstructure, such as (i) possibility of generating textured material due to consolidation of milled powder via hot roll sintering (HRS), and (ii) relatively lesser contrast in the grain-size of the core and the shell regions in the harmonic-structured Ti prepared from small-sized powder particles via jet-milling followed by spark plasma sintering. Therefore, the above mentioned aspects require a careful consideration to enhance our understanding about the properties and performance of harmonic structured metals and alloys with HCP crystal structure.

The objective of the present work is to prepare and evaluate bulk harmonic structured pure Ti in view of the issues discussed above, including processing, microstructure, mechanical properties, and deformation behavior. The processing involved mechanical milling of pure Ti powders followed by spark plasma sintering of milled powders. The results related with the microstructural evolution at various stages of processing and the mechanical properties of the harmonic structured Ti are presented and discussed, wherein the processing-structure-properties correlation has been attempted to be made. An attempt has also been made to unveil the deformation behavior of harmonic structured Ti through numerical simulation as well as experimental results. Therefore, various aspects dealing with the microstructural features, processing methodology, deformation behavior, and mechanical properties of harmonic structure design are discussed in the present work.

2. Experimental Procedure

The present work involved usage of pure Ti powders prepared by plasma rotating electrode process (PREP), having particle size in the range of 150–212 μm. The PREP Ti powder was mechanically milled (MM) in a planetary ball mill (Fritsch P-5) using steel vials and balls under argon gas atmosphere having ball-to-powder ratio 1.8. The milling was carried out at a rotation speed of 200 rpm for 90 ks (25 h), 180 ks (50 h), 270 ks (75 h), and 360 ks (100 h). Subsequently, the milled powders were consolidated by spark plasma sintering (SPS) at 1073 K (800°C) under vacuum for 1.8 ks at 50 MPa applied pressure, using a graphite die with 15 mm internal diameter. The microstructural characteristics of the initial powder, MMed powder, and the sintered compacts were observed by scanning electron microscope (SEM), electron backscattered diffraction (EBSD) technique, and transmission electron microscope. The specimen for TEM observations were prepared by focused ion beam (FIB) method. The mechanical properties of the materials were evaluated by hardness measurements and tension tests. An average of 25 measurements was considered as the representative average hardness of the material. The tensile tests were carried out at a strain rate of 5.6×10^{-4} s^{-1} using sub-size specimens with gauge dimensions 3 mm (length) × 1 mm (width) × 1 mm (thickness).

Numerical simulations were carried out to understand and elaborate the deformation behavior and the reason for such an excellent strength-ductility combination in the harmonic structured materials. The multiscale Finite Element (FE) Modeling was applied to a heterogeneous harmonic structure Ti with a specific topological distribution of UFG and CG areas. The harmonic structure in the unit cubic element was modeled as body centered cubic type structure wherein the CG core region was positioned at the corners of the cubic unit element. The detailed methodologies of the modeling procedure are provided elsewhere.[21–24] The averaged macroscopic properties of heterogeneous harmonic microstructure were obtained using the concept of a representative volume element (RVE). An RVE is defined as a part extracted from the complete microstructure and it acts as a representative of the complete microstructure. In the present work, a truncated octahedron has been used to constitute the RVE of the harmonic-structure model for the FE analyses owing to its efficient space-filling characteristic (Fig. 2a). The arrangement of the truncated octahedron can form a bi-truncated cubic honeycomb, which can be realized as a body-centered cubic lat-

tice.[25–27] Figure 2a also shows the harmonic-structure material composed of the CG cores and UFG shell. Because of efficient space filling, this model can maintain almost the same thickness as the actual object throughout the shell. In contrast to this research, a sphere is often chosen as the shape of an inclusion in FE models, in which the range of the volume fraction is limited. Figure 2b shows the mesh for an RVE of the pure Titanium with harmonic-structure design.

In the present research, the hexahedral mesh has been selected considering the regular shape of a truncated octahedron, together with the reduced error and a smaller number of elements associated with the hexagonal mesh as compared to tetrahedral mesh in FE methods for numerical simulation. An isotropic elastoplastic constitutive model based on Hooke's elasticity and Von Mises-type plasticity has been applied for the CG and UFG phases in this study. The same elastic constants of Ti were used for both CG and UFG phases. A Young's modulus of 100 GPa and Poisson's ratio of 0.3 were used for pure Ti for numerical simulations. Also, a UFG-shell/CG-core fraction of 0.27 was employed in the present work. The grain size of the UFG shell and CG core were considered as 2 μm and 15 μm, respectively, which are very close to the average values of the experimentally obtained harmonic Ti compacts. The detailed procedure to estimate the true stress-true strain curve of the CG and UFG parts of harmonic structure, which is used to in FE simulations, is provided elsewhere.[27]

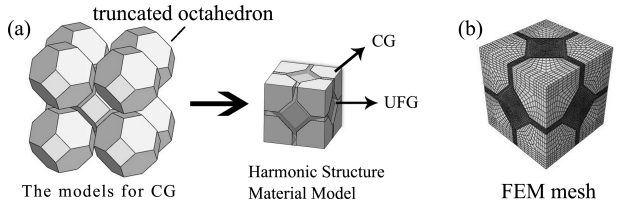

Fig. 2 (a) Harmonic-structure model consisting of truncated octahedrons and (b) FE model discretized by hexahedral elements of harmonic structure.

3. Results and Discussion

3.1 Morphology and microstructure of milled titanium powders

The effect of controlled mechanical milling on the morphology and microstructure of the powders, which are used to create harmonic structure, is illustrated in Figs. 3 and 4, respectively. Figure 3 shows the morphology of the PREP Titanium powder particles milled for 0 ks (IP), 90 ks (MM90), 180 ks (MM180), 270 ks (MM270), and 360 ks (MM360). It can be noticed that the shape of the PREP Titanium powder particles distorted as a result of controlled milling and the extent of distortion in the shape of the spherical PREP powder particles increased with increasing milling time. However, it would be worth mention that the mechanical milling was carried out in such a controlled manner that the powder particles did not either crushed or fragmented and the overall shape of the powder particle remained unaffected. The morphological features of the milled powder particles are a clear evidence of the fact that the titanium powder particles were subjected to severe plastic deformation in a very controlled manner. A closer observation of the morphology of the deformed surface also indicate a very ductile nature of the titanium powder particles.

Figure 4 shows the microstructure of the cross-section of PREP Titanium powder particles milled for 0 ks (IP), 90 ks (MM90), 180 ks (MM180), 270 ks (MM270), and 360 ks (MM360). It can be clearly observed that the controlled mechanical milling led to the formation of feature-less "shell-like" region near the surface of the powder particles. It can also be observed that the width of the shell region increased with increasing milling time. The previous work on different types of metals and alloys has demonstrated that the appearance of such a featureless shell-like region corresponds to the formation of severely deformed nanocrystalline region near the surface of the spherical powders due to controlled mechanical milling. Therefore, in the present case of pure Ti powders also, the controlled mechanical milling leads to se-

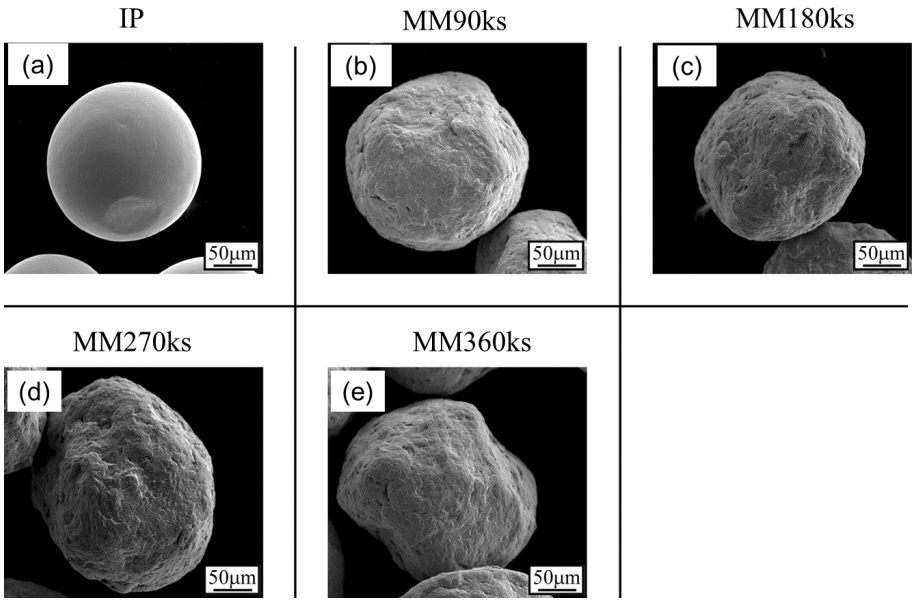

Fig. 3 Morphology of the PREP Ti powder milled for (a) 0 ks, (b) 90 ks, (c) 180 ks, (d) 270 ks, and (e) 360 ks.

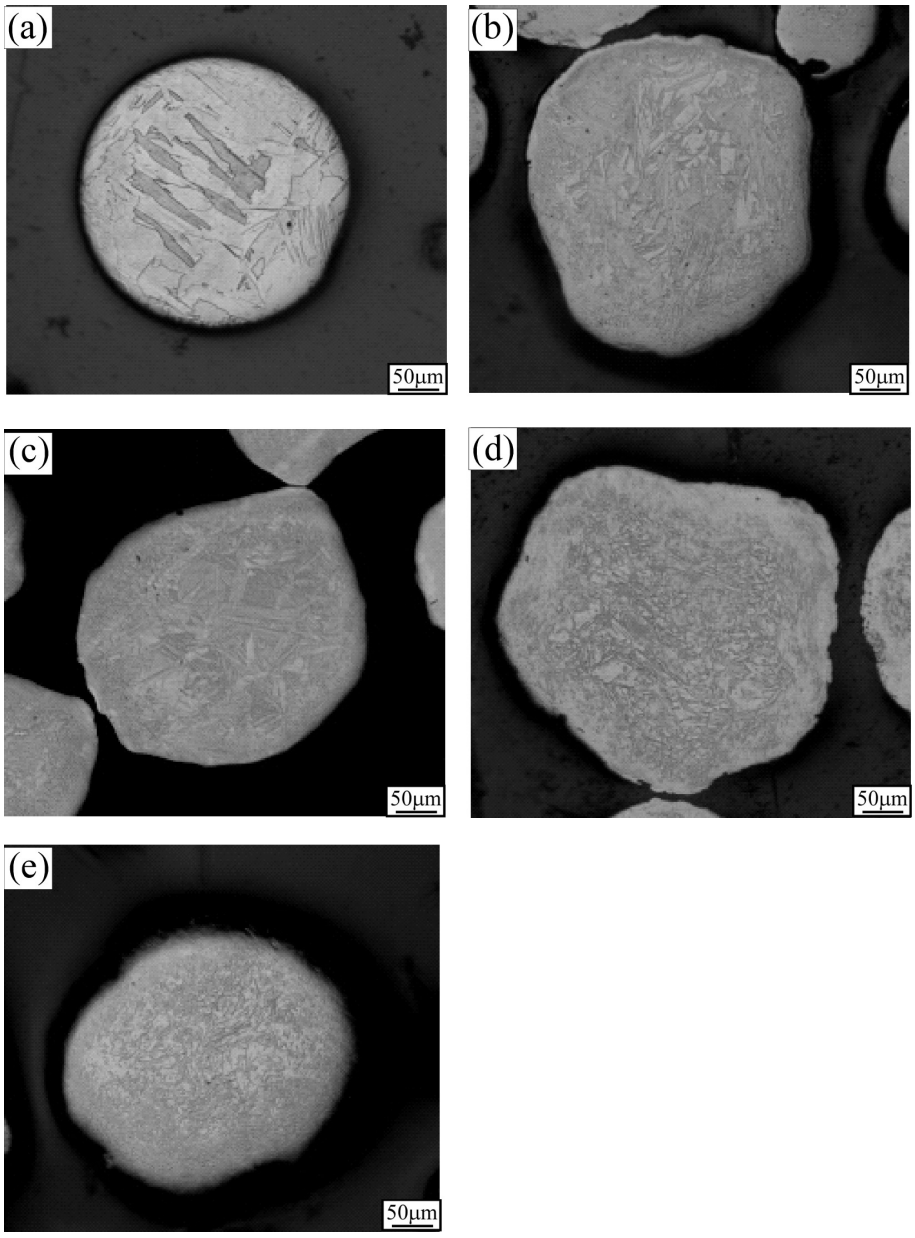

Fig. 4 Microstructure of the PREP Ti powder milled for (a) 0 ks, (b) 90 ks, (c) 180 ks, (d) 270 ks, and (e) 360 ks.

lective severe plastic deformation of the powder particles wherein the outer, i.e. near-surface, regions of the particles undergo severe plastic deformation whereas the inner parts remains relatively unaffected. Based on its appearance, the severely deformed outer part with nanocrystalline structure is commonly referred as "shell" whereas the inner un-deformed CG region is referred as "core". However, it would be worth mention that the inner core region does not remain absolutely unaffected by the severe plastic deformation infused to the near-surface region of the powder particles. Infact, the inner part is also affected by the controlled milling, leading to the infusion of plastic deformation up to the center of the powder particles, as shown in Fig. 4.

For more clarity, the microstructure of the cross-section of PREP powder milled for 360 ks, which illustrates the microstructure of the milled powders after the controlled milling, is shown in Fig. 5. The effect of plastic deformation in the inner part can be clearly observed in Fig. 5. Clearly, the milled

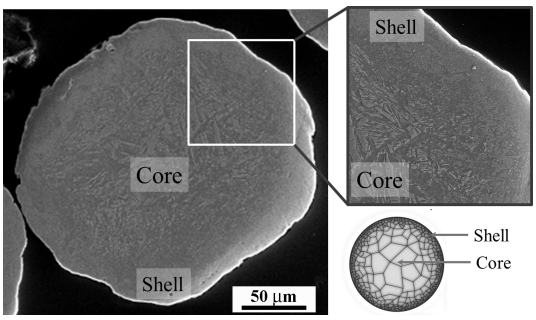

Fig. 5 Microstructure of the cross-section of PREP Ti powder particle milled for 360 ks.

powder particles consist of bimodal grain size distribution wherein severely deformed nano-crystalline shell region encapsulates the un-deformed/less-deformed CG microcrystalline core region. However, it would also be worth point out

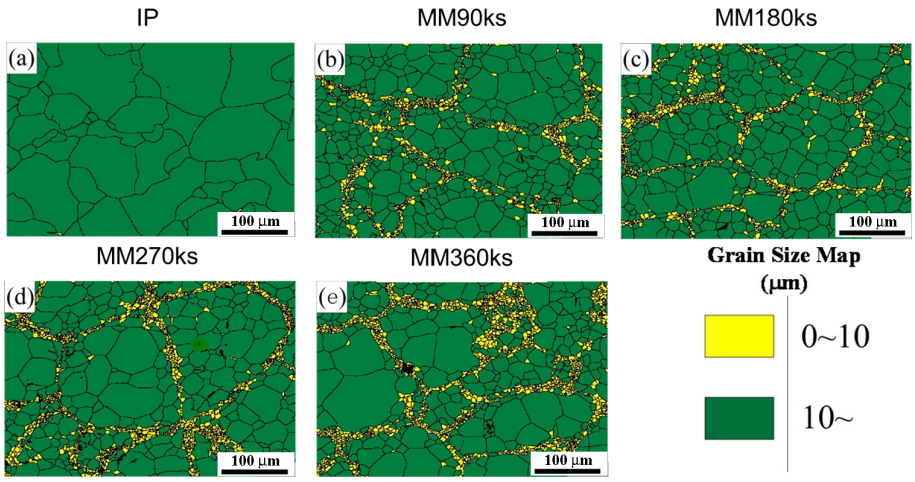

Fig. 6 Microstructure of sintered Ti compacts prepared from powder milled for various time periods: (a) 0 ks, (b) 90 ks, (c) 180 ks, (d) 270 ks, and (e) 360 ks.

Table 1 Volume fraction of fine-grained shell region in sintered Harmonic Titanium compacts.

	IP	MM90ks	MM180ks	MM270ks	MM360ks
Volume Fraction of Shell Area (%)	0.0	11	12	14	16

that there exists a gradient of extent of plastic deformation from surface toward the center of each and every milled powder particle. Ofcourse, the extent of gradient of plastic deformation depends on the nature of the material.

3.2 Microstructure of sintered titanium compacts

The milled powders were consolidated by SPS at 1073 K. Figure 6 shows the microstructure of the sintered compacts prepared from un-milled initial and milled PREP Titanium powders having bimodal grain size distribution. It can be observed that all the sintered compacts prepared from milled powders exhibit a unique microstructure having bimodal grain size distribution together with a typical topological distribution of fine-grained (FG) and CG areas, wherein FG areas (grain size < 10 μm) form an interconnected three dimensional network surrounding CG regions (grain size > 10 μm). This peculiar microstructural design is referred as "Harmonic Structure Design".[15–20] From Fig. 6, apart from bimodal structure evolution, it can also be noted that the average grain size of the CG core region is significantly smaller that of the CG IP sintered compacts. Furthermore, it can also be observed that there is a grain size gradient from UFG shell region towards the CG core region. Moreover, Table 1 shows that there was only slight increment in the FG shell region with increasing milling time. Nevertheless, it can be clearly noted that the width and continuity of the FG shell region increased with increasing milling time.

Such a typical microstructural evolution in the sintered harmonic structured Titanium compacts can be related directly with the microstructural characteristics of the milled powder particles, wherein the FG and CG areas are derived from the severely deformed "shell" and CG "core" regions, respectively, of the milled powders. It has been already demonstrated that the width/thickness of the severely deformed FG shell area increases with increasing milling time. As a result, thickness and volume fraction of interconnected FG shell increased with increasing milling time in the harmonic structured compacts. However, it would be worth mention that, in the present case, the increment in the volume fraction of shell region with increasing milling time is not as high as it was found in case of other metals and alloys. Especially, alloys exhibited higher amount of retention of FG shell region as compared to pure metals. Such a difference in the microstructural evolution can be attributed to the different mechanism of inhibition of grain growth in pure metals and alloys during sintering of milled powder particles.

The thermal stability of nanocrystalline structure, especially restricting grain growth during sintering of milled nanocrystalline/nano-sized high purity elemental powders at elevated temperatures, has been an important issue from engineering application point of view. In fact, attempts of achieving nanocrystalline structure in pure metals after sintering at elevated temperatures have proved unsuccessful in majority of the cases. Interestingly, the investigations on the thermal stability of nanocrystalline materials have demonstrated that a significant grain growth occurs in some of the pure metals even at room temperature, e.g. Al, Cu, Mg, Pb, Pd, and Sn.[28–31] However, at the same time, it was observed that the thermal stability of the nanocrystalline grains in the single phase metallic systems can be increased via reducing grain boundary mobility of the nanocrystalline grains through incorporating fine-sized dispersed second phases and grain boundary segregations, as demonstrated by introducing nano-sized nitride, oxide, and oxynitride phases in Al, Zn, Ni, and Fe based systems through cryomilling of pure metal powders in liquid nitrogen media.[32–37] Furthermore, some other investigations also have demonstrated that the presence of grain boundary segregation, solute drag, impurities, second phase drag, pore drag and chemical ordering lead to significantly enhanced thermal stability of nanocrystalline materials via a drag-force mechanism on the grain boundaries.[38–46] Similarly, in case of pure Ti, enhanced thermal stability of nanocrystalline structure was also observed in case of milled pure Ti powders, in liquid nitrogen as well as nitrogen gas mediums, after sintering at elevated temperatures.[46,47] It was demonstrated that the presence of nanosized nitrides and oxides, together with the segregation of nitrogen and oxygen, on

the grain boundaries was extremely effective in achieving stable nanocrystalline structure in pure Ti. Furthermore, it was also suggested that a combination of higher recrystallization rate and restricted grain growth leads to relatively smaller grain sizes.

As demonstrated before, in case of harmonic structure, the unique bimodal microstructure is derived from the milled powder particles with severely accumulated plastic deformation in the near-surface shell region and relatively less deformed inner core regions. In fact, the plastic deformation generates a smoothly decreasing gradient of accumulated plastic strain from surface towards the center of each and every powder particle. As a result, during sintering of powders at elevated temperatures, rate of recrystallization varies owing to this strain gradient, i.e. relatively higher number of nuclei/grains per unit volume are formed near the severely deformed surface regions as compared to the inner regions. In fact, there is a possibility that the inner regions may undergo only recovery and grain growth due to lack of sufficient amounts of accumulated plastic strain required for triggering recrystallization. Nevertheless, in case of alloys, it appears that the grain growth in the shell region is severely restricted owing to the presence of large amounts of solutes and second phase particles which retard the grain boundary migration. On the other hand, in case of pure metals, there is no such availability of any second phase particles or solutes which could stabilize the recrystallized FG structure in the shell region. However, as demonstrated in the present case of pure Ti also, pure metals forms a very thin layer of FG shell region.

It is well known that some amounts of oxides and/or nitrides, depending upon the method of preparation of powders, are always present on the surface of the powders. Moreover, there is always a chance of introduction of a little amount of oxygen in the milling vials despite having strict control during loading. It appears that these impurities get introduced in the outer layer of the metal powder during milling. Furthermore, there is also a possibility of introduction of a slight contamination/impurities in the surface layer of the powders from the milling vial and balls. It appears that a very high rate of recrystallization together with the presence of these impurities lead to a thin layer of FG shell in case of pure metals, as observed in the present case of pure Ti also (Fig. 6). It is also worth mentioning that the experimental evidences suggested that the gradient of strain accumulation is more distinct and higher in case of alloys as compared to pure metals due to higher strain hardenability of alloys. As a result, a distinct shell regions is formed in the alloy systems and it increases with increasing milling time. In case of pure elemental powders, the intensity of effect of plastic deformation reaches to the inner core of the relatively ductile pure elemental powders (Fig. 4), leading to overall relatively finer recrystallized grains in the core of the harmonic structured pure metals as compared to that of the compacts prepared from un-milled as received powders (Fig. 6).

3.3 Mechanical properties

Figure 7 illustrates the effect of milling time on the mechanical properties of harmonic structured pure Titanium. Figure 7a shows the engineering stress – engineering strain curves of Ti specimens having CG homogeneous as well as bimodal harmonic microstructures. Also, Fig. 7b illustrates the variation of yield strength and tensile strength with increasing milling time. It can be clearly observed that the creation of bimodal harmonic structure in pure Ti resulted in considerably higher yield strength and ultimate tensile strength as compared to their homogeneous CG counterparts. Moreover, it can also be observed that the improvement in the strengths was achieved without any significant reduction in the uniform deformation limit and total strain-to-fracture of the material. Figure 8 shows the relative integrated area under the stress-strain (S-S) curves of the harmonic structured compacts prepared from powders milled for different periods of time, with respect to the integrated area under the S-S curve of specimens from sintered IP powder compacts. Since the integrated area under the S-S curve is considered as an indicator of the "static" toughness of a metallic material, the relative area under the S-S curve can be treated as a change in the toughness of pure Ti compacts as a result of the creation of harmonic structure. It can be observed that the apparent toughness of the Ti compacts increased significantly, as high as 35%, as a result of formation of harmonic structure. Therefore, the above results clearly demonstrated that the bimodal harmonic structure is extremely effective in achieving improved toughness in the most of the strategic structural materials. The increasing strength values with increasing milling time, as shown in Fig. 7, appears to be related with the increased volume fraction and the continuity of the FG shell area with increasing milling time.

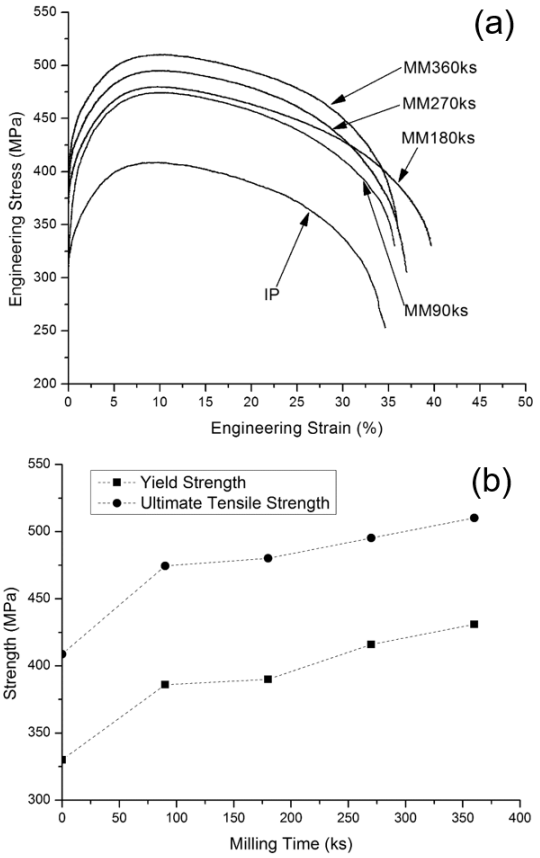

Fig. 7 Effect of milling time on the mechanical properties of harmonic Titanium: (a) Representative Engineering Stress- Engineering Strain curves, (b) Yield Strength and Ultimate Tensile Strength.

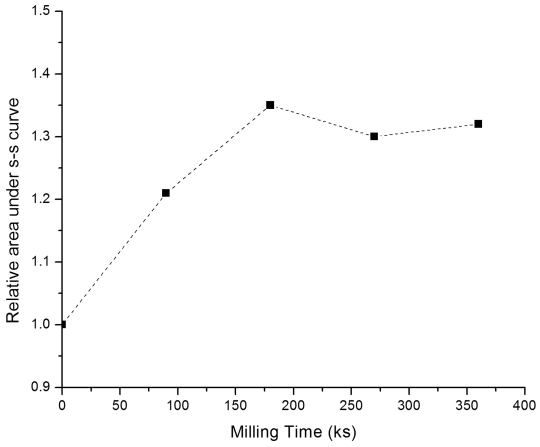

Fig. 8 Relative area under the stress-strain curves of the sintered compacts with increasing milling time. Values have been optimized with reference to specimens from initial powder compacts.

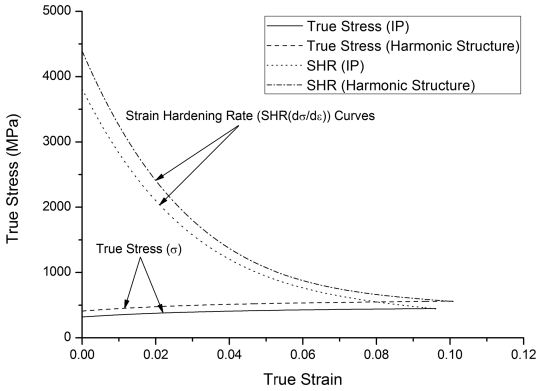

Fig. 9 True stress- true strain curves, together with their corresponding strain hardening rate (SHR) curves of the pure Titanium compacts with heterogeneous harmonic as well as homogeneous coarse-grained microstructure.

3.4 Deformation behavior

Figure 9 shows the true stress- true strain curves, together with their corresponding strain hardening rate (SHR, $\theta = (d\sigma/d\varepsilon)$) curves of the pure Titanium compacts with heterogeneous harmonic as well as homogeneous CG microstructure. It can be observed that, in general, the strain hardening rate decreases relatively rapidly in the early stages of deformation with increasing true strain, followed by an extremely small decreasing rate until the SHR curves crossover the true stress–true strain curves at the point of plastic instability, i.e., $d\sigma/d\varepsilon = \sigma$, and the necking starts thereafter. It can be observed that the harmonic and CG specimens, both, exhibit more or less similar overall macroscopic deformation behavior. However, it is interesting to note that the range of uniform plastic deformation extended to higher strain values for harmonic structure. Moreover, it can also be noticed that the SHR of bimodal harmonic structured Titanium remains relatively higher as compared to that of homogeneous CG specimens within the limit of uniform plastic deformation. However, it would also be worth mentioning that the difference in the SHR of the harmonic and homogeneous CG titanium continuously decreased with increasing tensile loading, and it became more or less comparable in the later stages of deformation, i.e. near the point of instability. These results clearly demonstrate that, in pure titanium, the harmonic structure facilitates not only higher strain hardening rate throughout the plastic deformation regime but also sustained uniform plastic deformation for an extended range of plastic deformation.

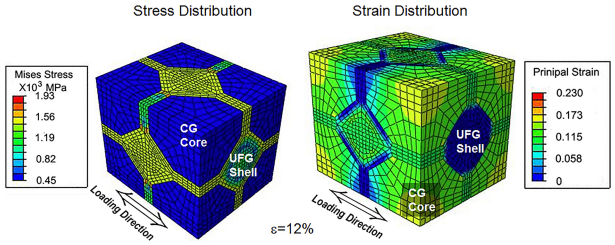

Fig. 10 Deformation behavior of harmonic structure through the simulation results showing the stress and strain distribution in the harmonic structured pure Titanium after approximately 12% deformation.

Figure 10 shows the numerical simulation results of harmonic structured pure Titanium, illustrating the stress and strain distribution in the specimens after approximately 12% deformation under applied unidirectional tensile loading. The simulation results clearly indicate that the FG shell regions are the high stress concentration areas. Particularly, the FG shell aligned along the tensile deformation direction exhibit relatively higher stress concentration as compared to that aligned perpendicular to the tensile deformation direction. However, the CG Core region does not show the evidence of accumulation of any significant stress concentration. From the numerical simulation results of strain distribution, it can be noted that the FG shell regions aligned perpendicular to tensile deformation axis do not show any evidence of accumulated strain concentration whereas some accumulated strain concentration can be observed in the shell region aligned parallel to tensile axis. However, it is interesting to note that the accumulated strain concentration "gradually" increased from the FG shell regions towards the center of the CG core regions. As a result, maximum accumulated strain at the center of the core regions is observed. At this juncture, it would be worth mentioning that the nature of distribution of the stress and strain accumulation were found to remain same, as demonstrated in the present case, even after varying the shell/core fraction in the harmonic structure (the results are not shown here). Furthermore, for the sake of preliminary comparison, the simulation results for the HS and inverse HS (with CG shell and UFG core) were also analyzed. The results indicated that, in contrast to HS, i.e. without the connection of the UFG phase, the inverse HS clearly experienced strain localization in the CG regions as the CG regions were forced to undergo more deformation due to the absence of stronger interconnected UFG areas. It is envisaged that such a strain localization in the inverse HS will lead to crack formation, leading to these regions to become the weakest regions in the inverse HS material. As a result, the HS materials may exhibit better ductility as compared to the inverse HS. However, the detailed discussion on the results of these aspects is beyond the scope of the present work and will be published in future.

The above results clearly indicate that the initial stages of the deformation and the strength of the harmonic structured

materials is governed by the deformation of interconnected network of the stronger FG shell regions. It appears that the three dimensional interconnected network acts as basic skeleton of the harmonic structure. As a result, the strength aspect during the deformation of the harmonic structured bulk material is governed by the deformation of stronger FG skeleton, leading to higher yield strength as compared to CG specimens. However, the strain accompanied by plastic deformation is not localized in the FG areas due to its inability to accommodate any large extent of strain. Most of the strain is accommodated by the CG core regions wherein the strain accumulation increases "gradually" from the shell/core boundary towards the center of the core. These results clearly demonstrate that the CG core regions accommodate the deformation-induced strain accumulation very efficiently without any localization, i.e. harmonic structure promotes uniform deformation. It appears that such a strain distribution is very effective in sustained work hardening up to large strain values, leading to higher strength values throughout the deformation process.

Based on the experimental and simulation results, the deformation behavior of the harmonic structured pure titanium can be explained in the following way. The relatively stronger FG "shell" can be considered as three dimensional interconnected "skeleton" of the microstructure. In such a scenario, the harmonic structured materials can be plastically deformed only when the plastic deformation is achieved in the stronger FG skeleton structure. Hence, the interconnected FG shell structure becomes area with high stress localization, and it dominates the early stages of deformation, leading to higher yield strength. Subsequently, to accommodate the overall shape change in the specimens due to plastic deformation, the well-arranged periodic CG core regions together with interconnected FG shell network also undergo a change in shape. However, the FG areas do not allow any significant amount of accumulation of localized strain owing to their inability to accommodate any large extent of strain in the form of dislocations and other defects. Since ductile/soft core areas are constrained by the stronger shell structure, these soft and ductile core regions also deform in order to accommodate the overall shape change of the shell structure. The subsequent deformation occurs in such a way that the continuity of the material is retained. To achieve this objective, the plastic strain is transferred towards the most ductile regions, i.e. center of the core regions, through the interface of CG/FG areas via a complex mode of deformation rather than pure tensile mode. The plastic deformation of the core also leads to the strain hardening, resulting in the higher strength values with increasing straining. It appears that such a complex deformation behavior results in sustained strengthening of harmonic structured titanium, leading to higher strength and delayed point of plastic instability as compared to CG structure. Hence, the gradient and periodic microstructure leads to an evolution of a complex and well targeted strain distribution in the harmonic structure during plastic deformation, which appears to be very effective in sustained work hardening up to large strain values leading to higher strength values throughout the deformation process.

4. Conclusions

Pure Ti compacts with unique bimodal harmonic structure were successfully prepared by an integrated approach based on controlled mechanical milling followed by spark plasma sintering. The controlled mechanical milling led to the formation of a peculiar UFG-Core/CG-Shell structure in the powder particles. Spark plasma sintering resulted in sintered compacts having a unique bimodal microstructure with a peculiar topological distribution of FG areas consisting of FG areas as interconnected three dimensional network surrounding CG regions. The creation of bimodal harmonic structure in pure Ti led to considerably higher yield strength, ultimate tensile strength, and apparent toughness as compared to their homogeneous CG counterparts. Such an improvement in strength was achieved without any loss of ductility. The experimental and numerical simulation results revealed that the initial stages of the deformation and strength of the harmonic structure is governed by the characteristics of the interconnected network of the FG shell regions. On the other hand, the extent of uniform deformation and overall ductility is governed by the ductile CG core region. The results also indicated that the harmonic structure promotes uniform deformation by avoiding strain localization during plastic deformation. It has been demonstrated that the accommodation of plastic deformation via gradual distribution of strain in the CG core areas is very effective in achieving sustained work hardening to a large strain values. These special characteristics of harmonic structure lead to higher strength values and uniform plastic deformation throughout the deformation process.

Acknowledgements

This research was supported by the Japan Science and Technology Agency (JST) under Collaborative Research Based on Industrial Demand "Heterogeneous Structure Control: Towards Innovative Development of Metallic Structural Materials", by the Grant-in-Aid for Scientific Research on Innovative Area, "Bulk Nanostructured Metals" through MEXT, Japan (contract No.22102004), and by the French National Research Agency in the framework of the "HighS-Ti project": ANR-14-CE07-0003. These supports are gratefully appreciated.

REFERENCES

1) N. Hansen: Scr. Mater. **51** (2004) 801–806.
2) M.A. Meyers, A. Mishra and D.J. Benson: Prog. Mater. Sci. **51** (2006) 427–556.
3) Y. Estrin and A. Vinogradov: Acta Mater. **61** (2013) 782–817.
4) Y. Saito, H. Utsunomiya, N. Tsuji and T. Sakai: Acta Mater. **47** (1999) 579–583.
5) R.Z. Valiev, R.K. Islamgaliev and I.V. Alexandrov: Prog. Mater. Sci. **45** (2000) 103–189.
6) R.Z. Valiev and T.G. Langdon: Prog. Mater. Sci. **51** (2006) 881–981.
7) A.P. Zhilyaev and T.G. Langdon: Prog. Mater. Sci. **53** (2008) 893–979.
8) Y. Wang, T. Jiao and E. Ma: Trans. JIM **44** (2003) 1926–1934.
9) S.K. Vajpai and R.K. Dube: J. Mater. Sci. **44** (2009) 129–135.
10) C. Suryanarayana and N. Al-Aqeeli: Prog. Mater. Sci. **58** (2013) 383–502.
11) Y. Wang, M. Chen, F. Zhou and E. Ma: Nature **419** (2002) 912–915.
12) D. Witkin, Z. Lee, R. Rodriguez, S. Nutt and E. Lavernia: Scr. Mater.

49 (2003) 297–302.
13) Y.M. Wang and E. Ma: Acta Mater. **52** (2004) 1699–1709.
14) G. Dirras, J. Gubicza, S. Ramtani, Q.H. Bui and T. Szilagyi: Mater. Sci. Eng. A **527** (2010) 1206–1214.
15) T. Sekiguchi, K. Ono, H. Fujiwara and K. Ameyama: Trans. JIM **51** (2010) 39–45.
16) C. Sawangrat, O. Yamaguchi, S.K. Vajpai and K. Ameyama: Trans. JIM **55** (2014) 99–105.
17) Z. Zhang, S.K. Vajpai, D. Orlov and K. Ameyama: Mater. Sci. Eng. A **598** (2014) 106–113.
18) M. Ota, S.K. Vajpai, R. Imao, K. Kurokawa and K. Ameyama: Trans. JIM **56** (2015) 154–159.
19) S.K. Vajpai, M. Ota, T. Watanabe, R. Maeda, T. Sekiguchi, T. Kusaka and K. Ameyama: Metall. Mater. Trans. A **46** (2015) 903–914.
20) Z. Zhang, D. Orlov, S.K. Vajpai, B. Tong and K. Ameyama: Adv. Eng. Mater. **17** (2015) 791–795.
21) I. Watanabe, D. Setoyama, N. Iwata and K. Nakanishi: Int. J. Plast. **26** (2010) 570–585.
22) I. Watanabe, A. Hosokawa and S. Tsutsumi: J. Smart Process **2** (2013) 119–122.
23) D. Setoyama, I. Watanabe and N. Iwata: Tetsu-to-Hagane **98** (2012) 290–295.
24) I. Watanabe and R. Ueji: Tetsu-to-Hagane **98** (2012) 283–289.
25) N. Chantarapanich, P. Puttawibul, S. Sucharitpwatskul, P. Jeamwatthanachai, S. Inglam and K. Sitthiseripratip: Comput. Math. Methods Med. (2012) Article ID 407805, 14 pages.
26) W.L. Yang, K. Peng, L.P. Zhou, J.J. Zhu and D.Y. Li: Comput. Mater. Sci. **83** (2014) 375–380.
27) H. Yu, I. Watanabe and K. Ameyama: Adv. Mater. Res. **1088** (2015) 853–857.
28) R. Birringer: Mater. Sci. Eng. A **117** (1989) 33–43.
29) R. Günther, A. Kumpmann and H.D. Kunze: Scr. Metall. Mater. **27** (1992) 833–838.
30) J. Weissmüller, J. Löffer and M. Kleber: Nanostr. Mater. **6** (1995) 105–114.
31) B. Huang, R.J. Parez and E.J. Lavernia: Mater. Sci. Eng. A **255** (1998) 124–132.
32) V.L. Tellkamp, S. Dallek, D. Cheng and E.J. Lavernia: J. Mater. Res. **16** (2001) 938–944.
33) J. He and E.J. Lavernia: J. Mater. Res. **16** (2001) 2724–2732.
34) F. Zhou, S.R. Nutt, C.C. Bampton and E.J. Lavernia: Metall. Mater. Trans. A **34** (2003) 1985–1992.
35) Y. Xun, E.J. Lavernia and F.A. Mohamed: Metall. Mater. Trans. A **35** (2004) 573–581.
36) V.L. Tellkamp, A. Melmed and E.J. Lavernia: Metall. Mater. Trans., A Phys. Metall. Mater. Sci. **35A** (2004) 2335–2343.
37) H.J. Höfler and R.S. Averback: Scr. Metall. Mater. **24** (1990) 2401–2406.
38) K. Boylan, D. Ostrander, U. Erb, G. Palumbo and K.T. Aust: Scr. Metall. Mater. **25** (1991) 2711–2716.
39) J. Eckert, J.C. Holzer and W.L. Johnson: J. Appl. Phys. **73** (1993) 131–135.
40) P. Knauth, A. Charai and P. Gas: Scripta Mater. Metall. **28** (1993) 325–330.
41) A. Kumpmann, R. Gunter and H.D. Kunze: Mater. Sci. Eng. A **168** (1993) 165–169.
42) C. Bansal, Z. Gao and B. Fultz: Nanostr. Mater. **5** (1995) 327–336.
43) L. He and E. Ma: Nanostr. Mater. **7** (1996) 327–339.
44) T.R. Malow and C.C. Koch: Acta Mater. **45** (1997) 2177–2186.
45) K.W. Liu and F. Muchlin: Acta Mater. **49** (2001) 395–403.
46) F. Sun, A. Zuniga, P. Rojas and E.J. Lavernia: Metall. Mater. Trans. A **37** (2006) 2069–2078.
47) T.D. Shen and C.C. Koch: Nanostr. Mater. **5** (1995) 615–629.